Supporting Information

Piperazine: A Promising Building Block for Aggregation-Induced Emission Materials

Tuokai Peng,[a] and Hui-Qing Peng*[a, b]

[a] State Key Laboratory of Chemical Resource Engineering, Beijing Advanced Innovation Center for Soft Matter Science and Engineering, Beijing University of Chemical Technology, Beijing 100029, China

[b] Guangdong Provincial Key Laboratory of Luminescence from Molecular Aggregates, South China University of Technology, Guangzhou 510640, China

*Corresponding Author: hqpeng@mail.buct.edu.cn (Hui-Qing Peng);

Table of contents

Materials and Methods

Materials.

Potassium hexafluorophosphate, 4-fluoronitrobenzene, pyridine 4-borate, iron powder and tetrakis-(triphenylphosphine)-palladium were purchased from Bide Pharmatech Ltd. 1,2-dibromoethane and piperazine were purchased from Inno-chem. Methyl iodide and 4-fluoroaniline were purchased from Energy-Chemical. Acetic acid and acid red 94 was purchased from Tokyo-Chemical-Industry. Aniline and 4-aminoanisole were purchased from Aladdin. Sodium carbonate, potassium carbonate and sodium sulphate were purchased form FuChen Technology Co., Ltd. All the commercially available reactants and reagents were used as received without further purification.

Instruments.

^{1}H and ^{13}C NMR spectra were obtained on a Bruker Advance III spectrometer in $CDCl_3$ and DMSO-d_6 using tetramethylsilane (TMS, δ = 0) as internal reference. UV-vis spectra, photoluminescence (PL) spectra, molar absorption values and fluorescence quantum yields (QY) were measured on a Shimadzu UV-2600i spectrophotometer and a Shimadzu RF-6000 spectrophotometer, respectively. High resolution mass spectrometry (HR-MS) measurements were performed on a Waters UPLC/Premier mass spectrometer. X-Ray singlecrystal diffraction data were collected on a Gemini E X-ray diffraction (Agilent, Oxford) with graphitemonochromator Mo-Kα (λ = 0.71073 Å) at 110 K. ROS assays were conducted by using a Xenon lamp (Microsolar300, Beijing Perfectlight). The quantum efficiencies were measured using an Edinburgh FS5 fluorescence spectrophotometer. ESR analysis was performed on a Bruker E 500 spectrometer.

Methods.

Molar absorption values (ε) were tested by UV-vis spectrophotometer and obtained according to the following equation:

$$\varepsilon = \frac{A}{cl}$$

A: absorption values; c: concentration; l: thickness of cuvette

Fluorescence quantum yields (QY) was tested on a spectrophotometer using quinine sulfate (1 μg / mL, Φ = 0.54) in diluted sulfuric acid (0.05 mM) as the standard substance.

Details of the X-ray crystallography

Single crystals of $C_{16}H_{18}N_2$ (**PA-H**) [exp_7878] were recrystallised from [solvents] mounted in inert oil and transferred to the cold gas stream of the diffractometer. Single crystals of $C_{16}H_{16}F_2N_2$ (**PA-F**) [exp_7770] were recrystallised from [solvents] mounted in inert oil and transferred to the cold gas stream of the diffractometer. Single crystals of $C_{18}H_{22}N_2O_2$ (**PA-OCH$_3$**) [exp_7936] were recrystallised from [solvents] mounted in inert oil and transferred to the cold gas stream of the diffractometer. Single crystals of $C_{16}H_{20}N_4$ (**PA-NH$_2$**) [exp_7935] were recrystallised from [solvents] mounted in inert oil and transferred to the cold gas stream of the diffractometer. Single crystals of $C_{18}H_{16}N_4$ (**PA-CN**) were recrystallised from [solvents] mounted in inert oil and transferred to the cold gas stream of the diffractometer. Single crystals of $C_9H_{10}N_2$ (**DMABN**) [exp_8224] were recrystallised from [solvents] mounted in inert oil and transferred to the cold gas stream of the diffractometer.

Crystal structure determination

Crystal Data. $C_{16}H_{18}N_2$ (**PA-H**), M =238.32, orthorhombic, a = 8.5407(8) Å, b = 8.5954(10) Å, c = 18.058(2) Å, U = 1325.6(3) Å^3, T = 239.95(10), space group Pbca (no. 61), Z = 4, μ(Mo Kα) = 0.071, 5437 reflections measured, 1295 unique (R_{int} = 0.0636) which were used in all calculations. The final wR(F_2) was 0.1396 (all data). Note :The I/sigma for the data drop below 3 at around 2 theta = 43. This is relatively low, but the best result that can be obtained, presumably due to the inherent properties of the material. $C_{16}H_{16}F_2N_2$ (**PA-F**) , M =274.31, monoclinic, a = 8.4198(9) Å, b = 5.6543(6) Å, c = 14.1818(11) Å, β = 101.313(9)°, U = 662.05(11) Å^3, T = 113.50(10), space group P21/c (no. 14), Z = 2, μ(Mo Kα) = 0.102, 2438 reflections measured, 1268 unique (R_{int} = 0.0328) which were used in all calculations. The final wR(F_2) was 0.1230 (all

data). $C_{18}H_{22}N_2O_2$ (**PA-OCH$_3$**), M =298.38, monoclinic, a = 7.7608(9) Å, b = 8.3096(9) Å, c = 11.9313(12) Å, β = 103.196(10)°, U = 749.13(14) Å^3, T = 117.4(3), space group P2$_1$/n (no. 14), Z = 2, μ(Mo Kα) = 0.087, 3046 reflections measured, 1434 unique (R_{int} = 0.0441) which were used in all calculations. The final wR(F_2) was 0.1233 (all data). $C_{16}H_{20}N_4$ (**PA-NH$_2$**), M =268.36, monoclinic, a = 12.305(6) Å, b = 5.6820(10) Å, c = 10.771(4) Å, β = 113.87(6)°, U = 688.7(5) Å^3, T = 117.7(6), space group P2$_1$/c (no. 14), Z = 2, μ(Mo Kα) = 0.080, 3631 reflections measured, 1319 unique (R_{int} = 0.0993) which were used in all calculations. The final wR(F_2) was 0.2899 (all data). Note : The I/sigma for the data drop below 3 at around 2 theta = 38. This is relatively low, but the best result that can be obtained, presumably due to the inherent properties of the material. $C_{18}H_{16}N_4$ (**PA-CN**), M = 288.35, monoclinic, a = 4.0268(2) Å, b = 11.5604(8) Å, c = 15.2182(10) Å, β = 93.647(5)°, U = 1413.51(16) Å^3, T = 117.1(8), space group P2$_1$/c (no. 14), Z = 2, μ(Mo Kα) = 0.084, 21049 reflections measured, 5435 unique (R_{int} = 0.0450) which were used in all calculations. The final wR(F_2) was 0.1051 (all data). $C_9H_{10}N_2$ (**DMABN**), M =146.19, monoclinic, a = 7.0765(5) Å, b = 7.5321(5) Å, c = 15.6647(16) Å, β = 88.918(6)°, U = 834.80(12) Å^3, T = 117.80(10), space group P2$_1$/c (no. 14), Z = 4, μ(Mo Kα) = 0.071, 3505 reflections measured, 1608 unique (R_{int} = 0.0698) which were used in all calculations. The final wR(F_2) was 0.1593 (all data). Note : The I/Sigma of 3 at 2 theta is of around 38. This is relatively low, but the best result that can be obtained, presumably due to the inherent properties of the material.

Computational details

The structures and for **PA-CN** have been studied via density functional theory (DFT) at their excited states. All studied geometries were optimized at TD [1-7] Lee–Yang–Parr gradient-corrected correlation functional hybrid functional [8, 9] (TD-B3LYP) with Grimme's DFT-D3(BJ) empirical dispersion correction [10] and the def2-SVP [11, 12] basis set level of theory by via Gaussian 09 D.01 [13]. The harmonic frequencies were performed at the same level to confirm that all studied structures as minima and transition states possess zero

and one imaginary frequency, i.e., they are located at the minima and saddle points on the potential energy surfaces, respectively All above calculations were performed at implicit solvent by solvation model based on solute electron density (SMD) [14], where water is for **PA-CN**.

Synthesis and Characterizations.

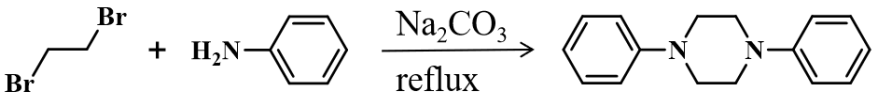

Scheme S1. The synthesis of **PA-H**.

Synthesis of PA-H: Dibromoethane (2 mL, 23.10 mmol), aniline (2 mL, 21.94 mmol) and Na_2CO_3 (3 g, 28.30 mmol) was added into a round bottom flask. The mixture was reflux for 6 h and was then cooled to room temperature. The organic layer was separated by extracting several times with dichloromethane (DCM). The organic phase was dried over anhydrous Na_2SO_4 and the solvent was evaporated under reduced pressure. Recrystallization from DCM/MeOH twice resulted in a white powder (1.12 g, yield = 43 %). The single crystal of **PA-H** was obtained in a tube by slowly evaporating in DCM at room temperature (colorless, square). ^{1}H NMR (400 MHz, $CDCl_3$), δ (TMS, ppm): 7.30 (dd, *J* = 8.4 Hz, 7.2 Hz, 4H), 6.99 (d, *J* = 8 Hz, 4H), 6.90 (t, *J* = 7.2 Hz, 2H), 3.35 (s, 8H). ^{13}C NMR (100 MHz, $CDCl_3$), δ (TMS, ppm): 151.2, 129.2, 120.0, 116.3, 49.4. HR-MS ($C_{16}H_{18}N_2$): m/z 239.1545 ($[M+H]^+$, calcd 239.1543).

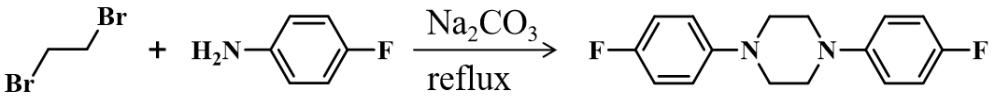

Scheme S2. The synthesis of **PA-F**.

Synthesis of PA-F: Dibromoethane (2 mL, 23.10 mmol), p-fluoroaniline (2 mL, 21.06 mmol) and Na_2CO_3 (3 g, 28.30 mmol) was added into a round bottom flask. After degas and refill with nitrogen for three times, the mixture was reflux for 6 h and was then cooled to room temperature. The organic layer was separated by extracting several times with DCM. The organic phase was dried over anhydrous Na_2SO_4 and the solvent was evaporated under reduced

pressure. Recrystallization from DCM/MeOH twice resulted in a white powder (1.1 g, yield = 38 %). The single crystal of **PA-F** was obtained in a tube by slowly evaporating in a mixed solvent of DCM/hexane = 1:1 (v/v) at room temperature (colorless, square). ^{1}H NMR (400 MHz, $CDCl_3$), δ (TMS, ppm): 7.02 ~ 6.92 (m, 8H), 3.27 (s, 8H). ^{13}C NMR (100 MHz, $CDCl_3$), δ (TMS, ppm): 157.4 (d, *J* = 237.8 Hz), 174.9 (d, *J* = 1.2 Hz), 118.2 (d, *J* = 7.5 Hz), 115.6 (d, *J* = 21.9 Hz), 50.5. HR-MS ($C_{16}H_{16}N_2F_2$): m/z 275.1366 ([M+H]$^+$, calcd 275.1355).

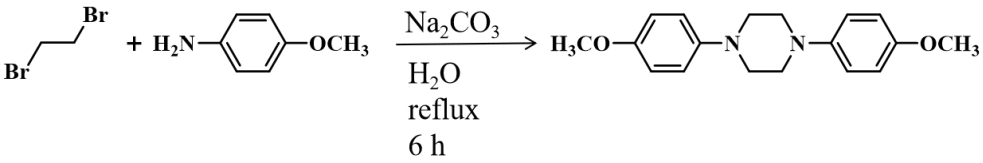

Scheme S3. The synthesis of **PA-OCH$_3$**.

Synthesis of PA-OCH$_3$: Dibromoethane (2 mL, 23.10 mmol), 4-methoxyaniline (2.86 g, 23.22 mmol), Na_2CO_3 (5 g, 47.17 mmol) and purified water (20 mL) was added into a round bottom flask. After degas and refill with nitrogen for three times, the mixture was reflux for 6 h and was then cooled to room temperature. The organic layer was separated by extracting several times with DCM. The organic phase was dried over anhydrous Na_2SO_4 and the solvent was evaporated under reduced pressure. Recrystallization from DCM/MeOH twice resulted in a white powder (1.52 g, yield = 44 %). The single crystal of **PA-OCH$_3$** was obtained in a tube by slowly evaporating in a mixed solvent of DCM/MeOH = 1:1 (v/v) at room temperature (colorless, square). ^{1}H NMR (400 MHz, $CDCl_3$) , δ (TMS, ppm): 6.96 (d, *J* = 8.8 Hz, 4H) , 6.86 (d, *J* = 8.8 Hz, 4H) , 3.78 (s, 6H) , 3.24 (s, 8H). ^{13}C NMR (100 MHz, $CDCl_3$), δ (TMS, ppm): 154, 145.7, 118.4, 114.5, 55.6, 51.0. HR-MS ($C_{18}H_{22}N_2O_2$): m/z 299.1754 ([M+H]$^+$, calcd 299.1755).

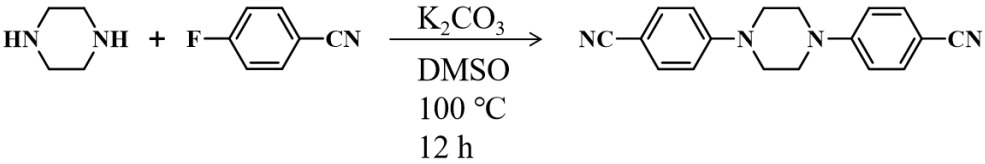

Scheme S4. The synthesis of **PA-CN**.

Synthesis of PA-CN: Piperazine (111.1 mg, 1.29 mmol) , p-fluorobenzonitrile (380.0 mg, 3.14 mmol) and K_2CO_3 (475.3 mg, 3.44 mmol) was added into a round bottom flask containing DMSO (10 mL). After degas and refill with nitrogen for three times, the mixture was reacted 12 h at 100 ℃ and was then cooled to room temperature. Water was injected into the mixture and a white precipitate appeared. The precipitate obtained was rinsed with a small amount of water to remove residual DMSO and recrystallized from DCM/PE to give a white powder (189 mg, yield = 51 %). The single crystal of **PA-CN** was obtained in a tube by slowly evaporating in a mixed solvent of DCM/Acetontrile = 1:1 (v/v) at room temperature (colorless, needle shape). ^{1}H NMR (400 MHz, $CDCl_3$), δ (TMS, ppm): 7.54 (d, *J* = 8.8 Hz, 4H) , 6.88 (d, *J* = 9.2 Hz, 4H) , 3.55 (s, 8H). ^{13}C NMR (100 MHz, $CDCl_3$), δ (TMS, ppm): 152.6, 133.6, 119.8, 114.2, 101.1, 46.7. HR-MS ($C_{18}H_{16}N_4$): m/z 289.1456 ([M+H]$^+$, calcd 289.1448).

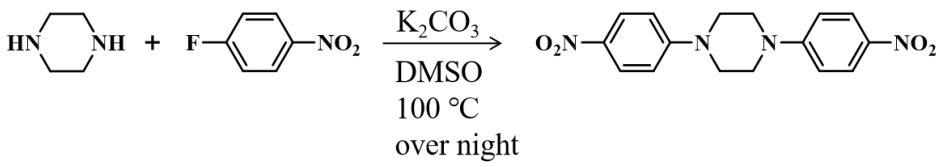

Scheme S5. The synthesis of **PA-NO$_2$**.

Synthesis of PA-NO$_2$: Piperazine (319.0 mg, 3.70 mmol), p-Fluoronitrobenzene (1.1 mL, 10.37 mmol) and K_2CO_3 (1.3 g, 9.42 mmol) was added into a round bottom flask containing DMSO. After degas and refill with nitrogen for three times, the mixture was reacted over night at 100 ℃ and was then cooled to room temperature accompanying with orange-yellow crystal like particles precipitated. The precipitate obtained was rinsed with a small amount of water to remove residual DMSO and recrystallized from DCM/PE to give a orange-yellow powder product (1.08 g, yield = 89 %). ^{1}H NMR (400 MHz, $CDCl_3$) , δ (TMS, ppm): 8.18 (d, *J* = 9.2 Hz, 4H) , 6.84 (d, *J* = 9.6 Hz, 4H) , 3.675 (s, 8H). HR-MS ($C_{16}H_{16}N_4O_4$): m/z 329.1238 ([M+H]$^+$, calcd 329.1245).

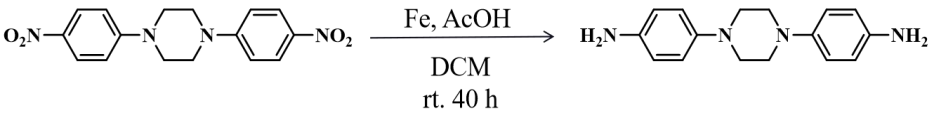

Scheme S6. The synthesis of **PA-NH$_2$**.

Synthesis of PA-NH$_2$: Acetic acid (10 mL), DCM (2 mL) and **PA-NO$_2$** (343 mg, 1.30 mmol) was added into a round bottom flask and mixed well. After iron powder (1.64 g) poured into the flask, the mixture was stirred 40 h at room temperature. An excess of Na_2CO_3 was then used to neutralize un-reacted acid. The mixture was extracted with ethyl acetate (EA) for several times, and the organic layer was separated. It was necessary to purify the mixture by column chromatography using EA/ethanol (50:1, v/v) as eluent and recrystallized from DCM/PE to give a yellow powder product (230 mg, yield = 66 %). The single crystal of **PA-NH$_2$** was obtained in a tube by slowly evaporating in a mixed solvent of DCM, EA, MeOH and ethanol at room temperature (yellow, needle shape). ^{1}H NMR (400 MHz, DMSO-d_6) , δ (TMS, ppm): 6.73 (d, J = 8.8 Hz, 4H), 6.51 (d, J = 8.4 Hz, 4H), 4.60 (br, 4H), 3.02 (s, 8H). ^{13}C NMR (100 MHz, DMSO-d_6), δ (TMS, ppm): 142.9, 142.6, 118.5, 115.3. HR-MS ($C_{16}H_{21}N_4$): m/z 269.1749 ([M+H]$^+$, calcd 269.1761).

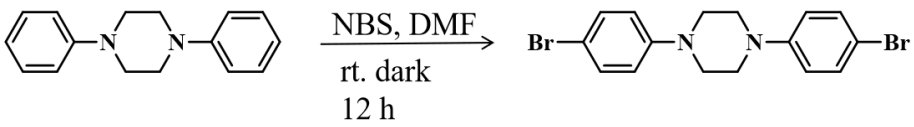

Scheme S7. The synthesis of **PA-Br**.

Synthesis of PA-Br: **PA-H** (1.02 g, 4.29 mmol) was added into a double port bottles containing DMF (10 mL) under condition of ice water bath. N-bromosuccinimide (NBS) (1.66 g, 9.33 mmol) was then dissolved in DMF (18 mL), which was slowly pipetted into the double port bottle. The mixture was stirred 12 h in dark at room temperature. Water was infused into the mixture and white deposit appeared. Then, it was purified by DCM:PE (1:2, v/v) on silica gel column to afford the pure **PA-Br** as white solid (1.02 g, yield = 60 %).

^{1}H NMR (400 MHz, $CDCl_3$), δ (TMS, ppm): 7.37 (d, *J* = 8.8 Hz, 4H), 6.84 (d, *J* = 8.8 Hz, 4H), 3.30 (s, 8H). HR-MS ($C_{16}H_{16}N_2Br_2$): m/z 396.9718 ([M+H]$^+$, calcd 396.9733).

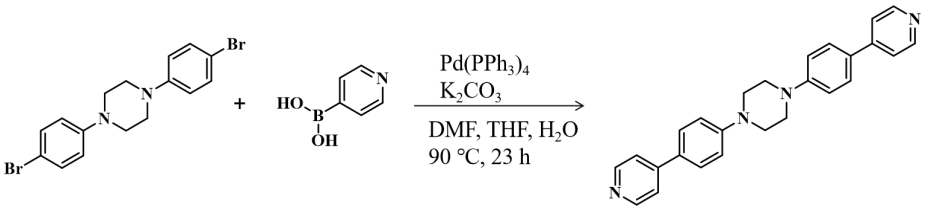

Scheme S8. The synthesis of **PA-Py**.

Synthesis of PA-Py: a mixture of **PA-Br** (365 mg, 0.92 mmol), 4-pyridylboronic acid (272 mg, 2.21 mmol), $Pd(PPh_3)_4$ (49 mg, 0.042 mmol), and an excess of K_2CO_3 (3.49 g) in mixed solution of DMF (12 mL), THF (30 mL) and water (12 mL) was stirred for 23 h at 90 °C under nitrogen atmosphere. After being cooled to the room temperature, the reaction mixture was extracted with DCM. The organic layer was washed with saturated NaCl solution, dried over anhydrous Na_2SO_4, and then evaporated in vacuum to dryness. The residue was purified by column chromatography with DCM/MeOH (20:1, v/v) to afford the pure **PA-Py** as yellow solid (112 mg, yield = 31 %). ^{1}H NMR (400 MHz, $CDCl_3$), δ (TMS, ppm): 8.61 (d, *J* = 6 Hz, 4H), 7.63 (d, *J* = 8.8 Hz, 4H), 7.51 (d, *J* = 6 Hz, 4H), 7.07 (d, *J* = 8.8 Hz, 4H), 3.47 (s, 8H). HR-MS ($C_{26}H_{24}N_4$): m/z 393.2083 ([M+H]$^+$, calcd 393.2074).

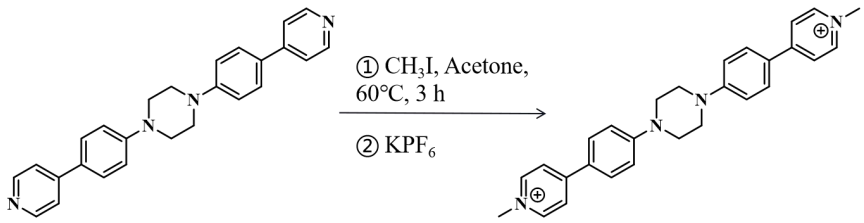

Scheme S9. Synthetic route of **PA-Py$^+$**.

Synthesis of PA-Py$^+$: A large excess of iodmethane (0.5 mL) was added into the acetone solution of **PA-Py** (32 mg, 0.082 mmol). The mixture was stirred at 65 ℃ for 3 h, where the color turned a deep yellow. After the mixture cooled to room temperature, the yellow precipitate was taken by filtration. Transfer the above yellow precipitate to a round bottom flask and add enough methanol to

dissolve it. Saturated aqueous KPF_6 (10 mL) was then added into the flask and reacted for 20 min at room temperature. Yellow powdered solid was obtained after the solvent was evaporated under reduced pressure and rinsed in a small volume of water (47 mg, yield = 80 %). ^{1}H NMR (400 MHz, DMSO-d_6), δ (TMS, ppm): 8.78 (d, J = 6.8 Hz, 4H), 8.37 (d, J = 6.8 Hz, 4H), 8.05 (d, J = 9.2 Hz, 4H), 7.16 (d, J = 8.8 Hz, 4H), 4.22 (s, 6H), 3.62 (s, 8H). ^{13}C NMR (100 MHz, DMSO-d_6), δ (TMS, ppm): 153.9, 153.4, 145.2, 130.0, 121.9, 114.7, 46.8, 46.3. HRMS ($C_{28}H_{30}N_4^{2+}$): m/z 211.1239 ([M+H]$^+$, calcd 211.1230).

ROS generation efficiency study.

A commonly used ROS indicator DCFH was employed to detect the overall ROS generation of **PA-Py$^+$** in solution under white light irradiation (24 mW·cm^{-2}). The fluorescence intensity of DCFH enhanced after reaction with ROS. In brief, the activated DCFH (c_{DCFH} = 5 μM) solution was mixed with **PA-Py$^+$** ($c_{PA\text{-}Py+}$ = 10 μM). Then the mixture was irradiated with white light at different time interval, and the PL spectra were obtained with excitation at 489 nm and emission was collected from 510 to 600 nm. The overall ROS generation efficiency (I/I_0 - 1) was determined by using the fluorescence intensity at 525 nm.

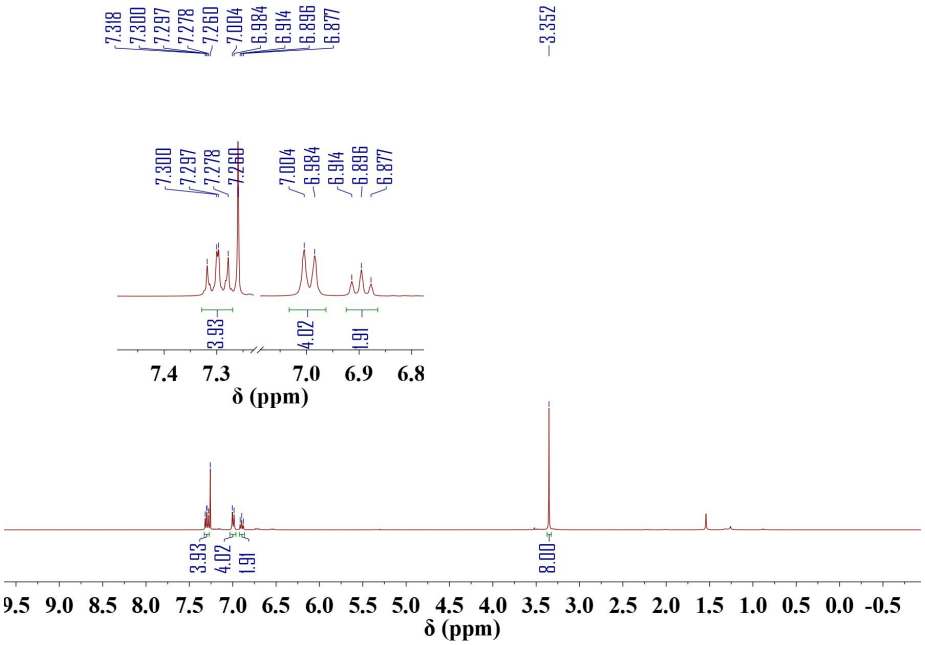

Fig. S1 ^{1}H NMR spectrum of **PA-H** in $CDCl_3$.

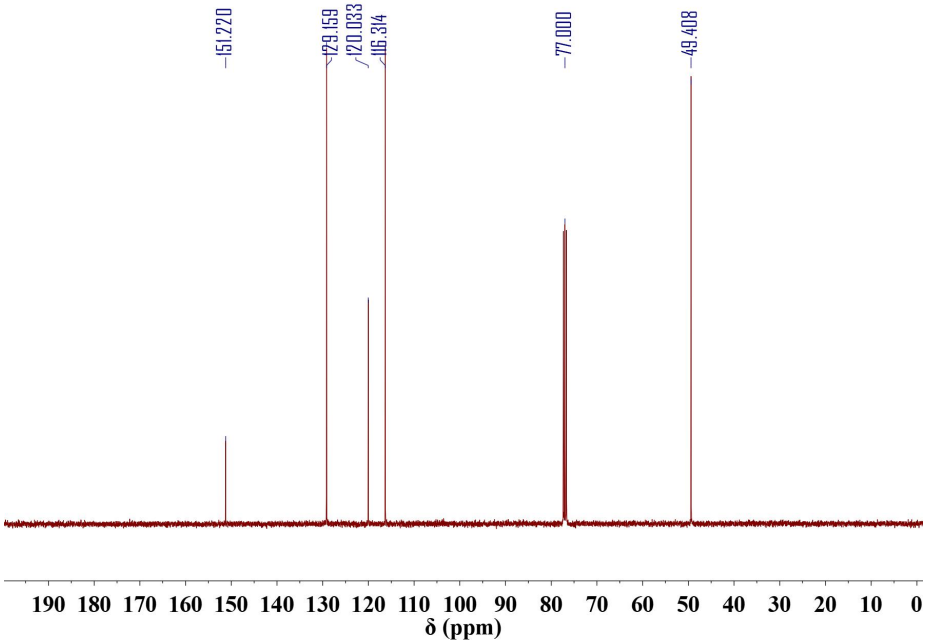

Fig. S2 ^{13}C NMR spectrum of **PA-H** in $CDCl_3$.

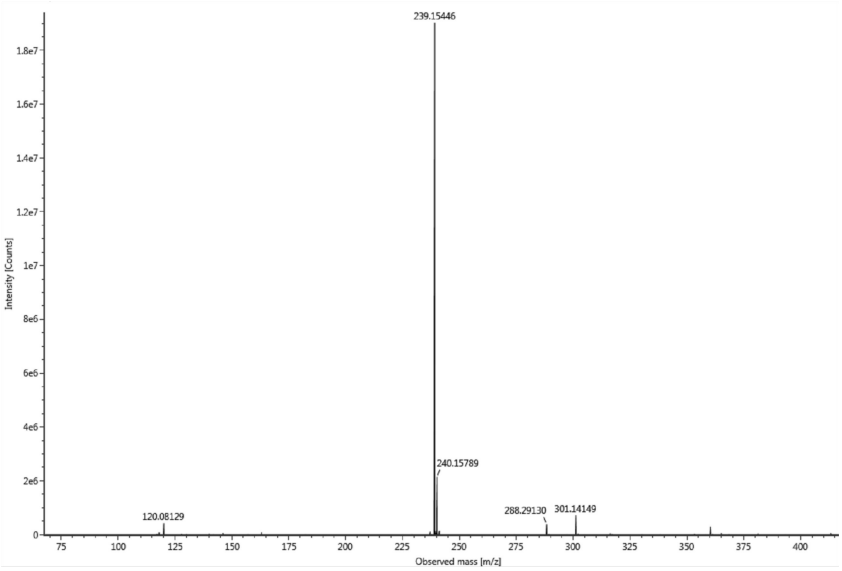

Fig. S3 HR-MS spectrum of **PA-H**.

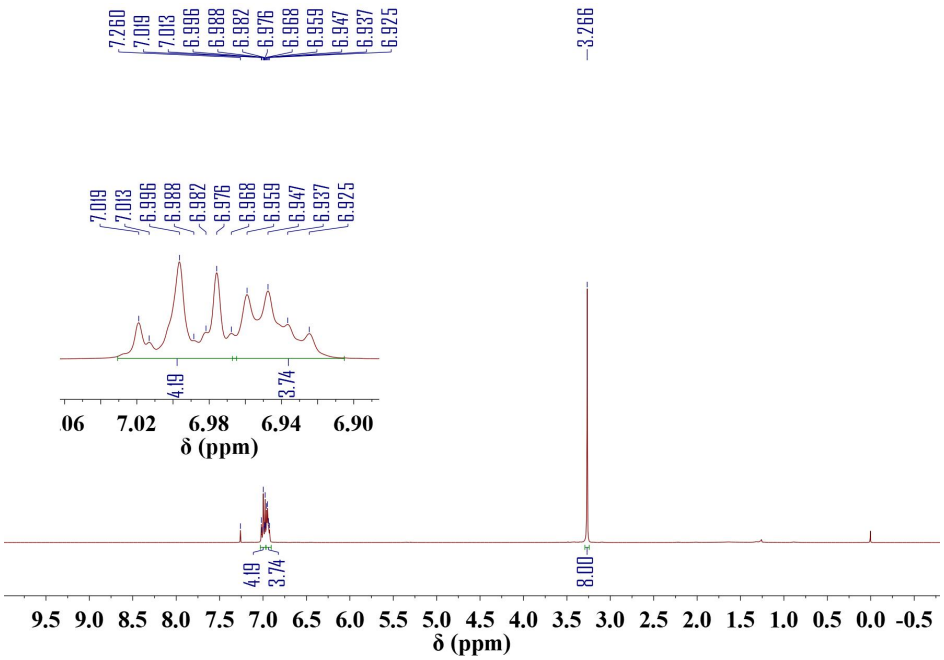

Fig. S4 ^{1}H NMR spectrum of **PA-F** in $CDCl_3$.

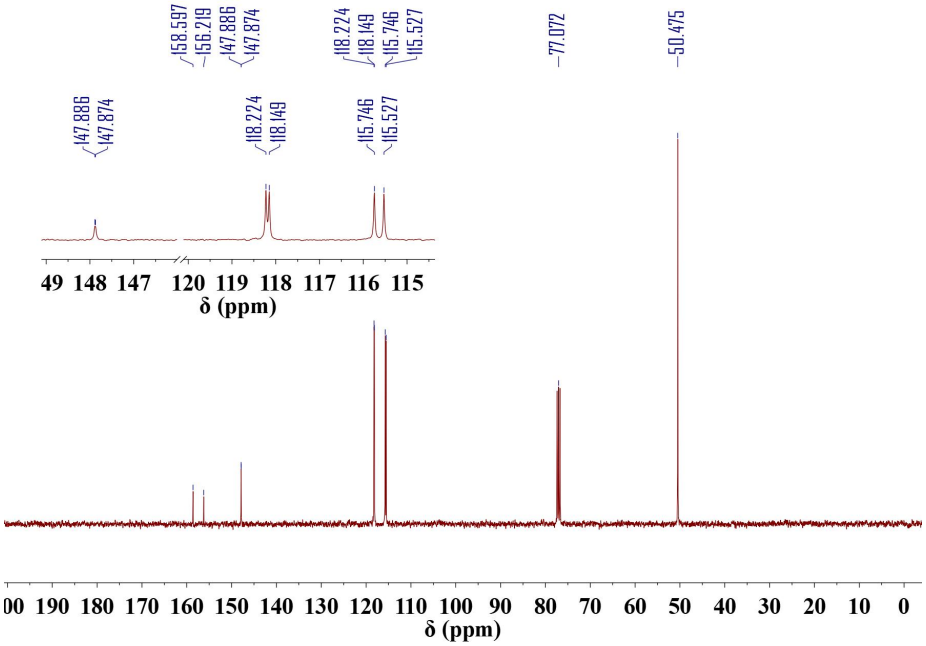

Fig. S5 ^{13}C NMR spectrum of **PA-F** in $CDCl_3$.

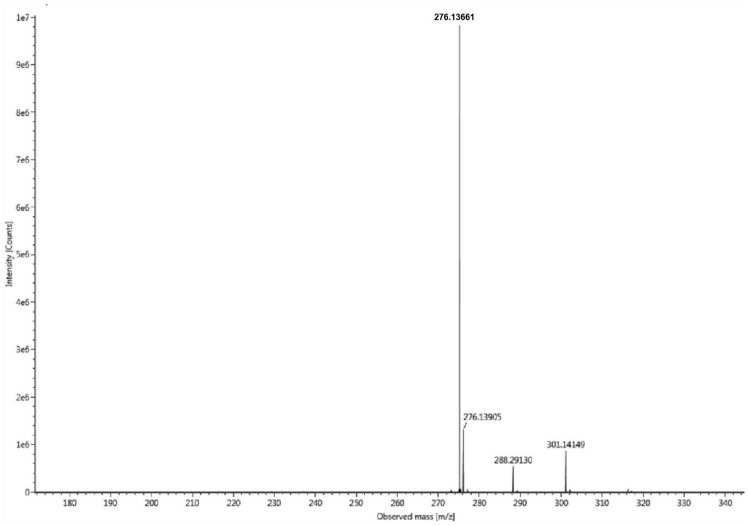

Fig. S6 HR-MS spectrum of **PA-F**.

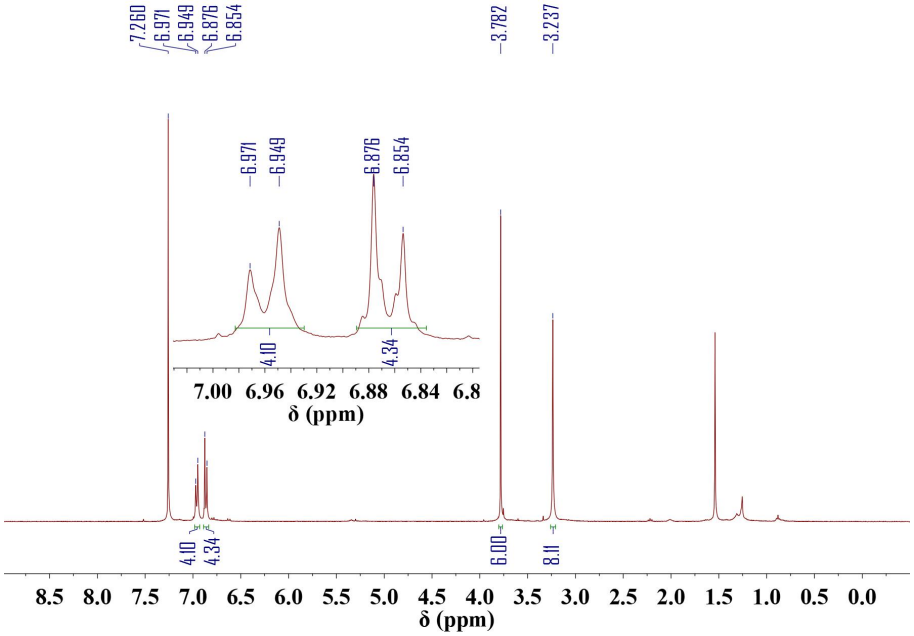

Fig. S7 ^{1}H NMR spectrum of **PA-OCH$_3$** in $CDCl_3$.

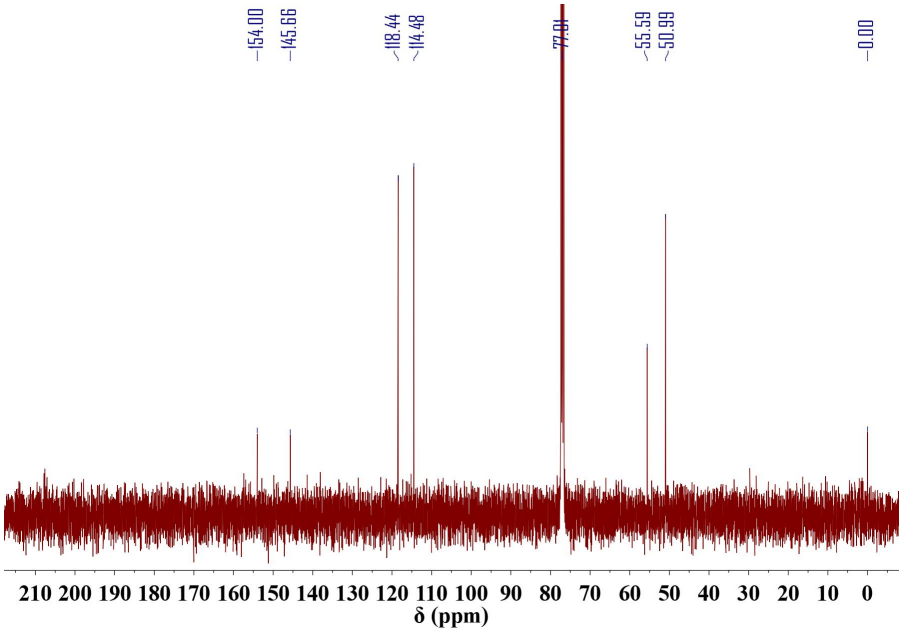

Fig. S8 ^{13}C NMR spectrum of **PA-OCH$_3$** in $CDCl_3$.

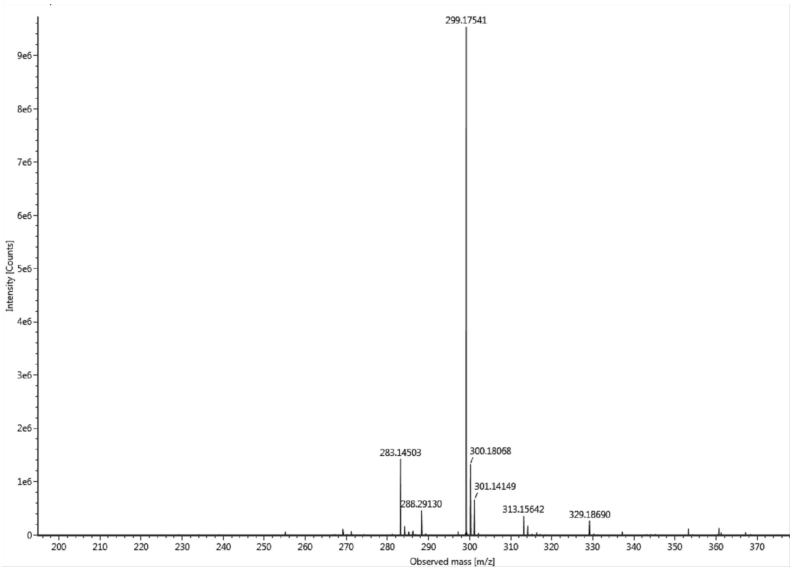

Fig. S9 HR-MS spectrum of **PA-OCH$_3$**.

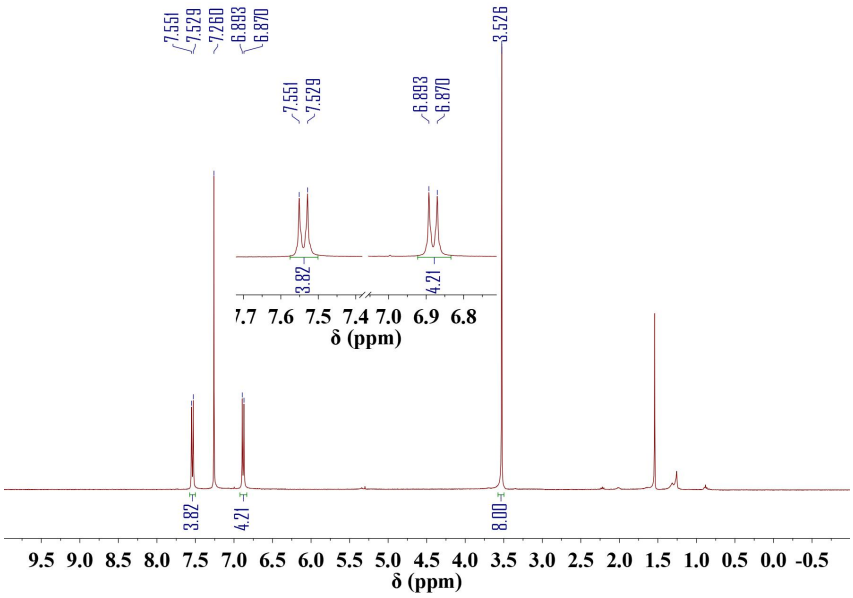

Fig. S10 ^{1}H NMR spectrum of **PA-CN** in $CDCl_3$.

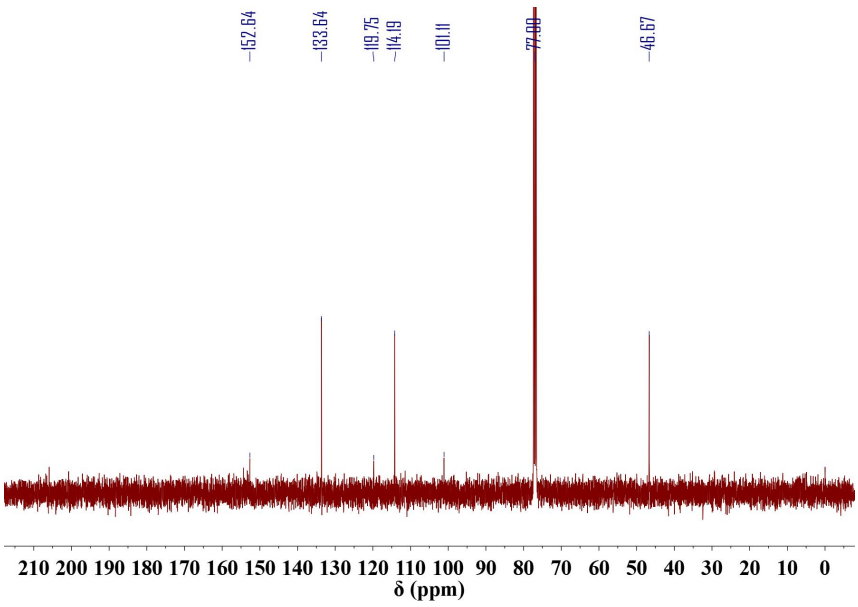

Fig. S11 ^{13}C NMR spectrum of **PA-CN** in $CDCl_3$.

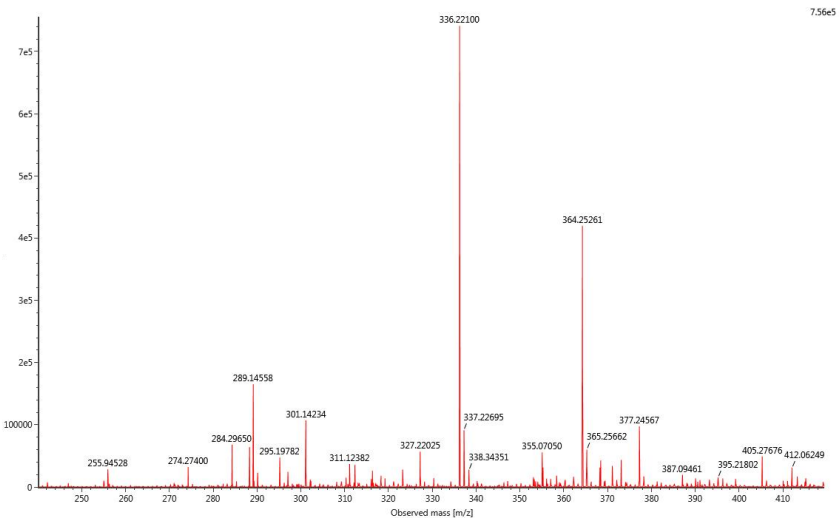

Fig. S12 HR-MS spectrum of **PA-CN**.

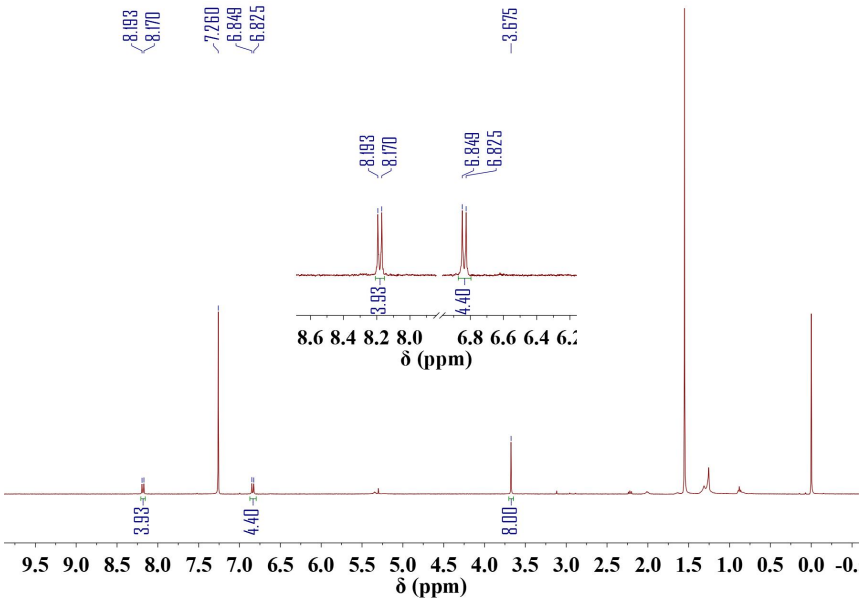

Fig. S13 ^{1}H NMR spectrum of **PA-NO$_2$** in $CDCl_3$.

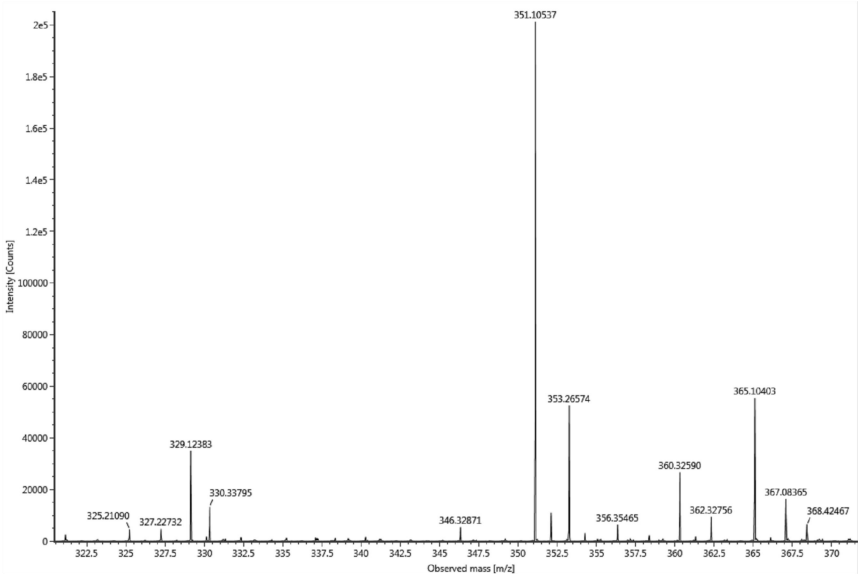

Fig. S14 HR-MS spectrum of **PA-NO$_2$**.

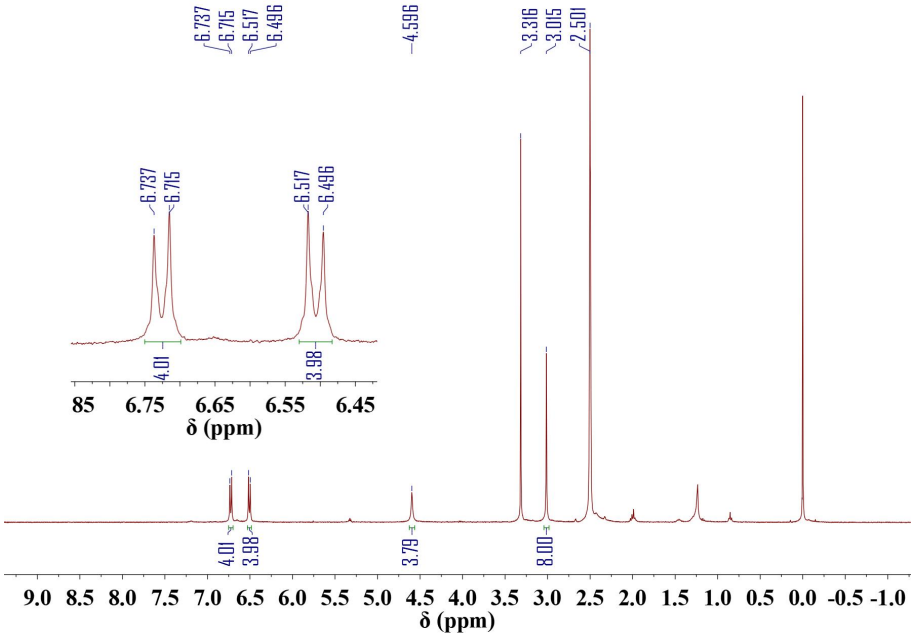

Fig. S15 ^{1}H NMR spectrum of **PA-NH$_2$** in DMSO-d$_6$.

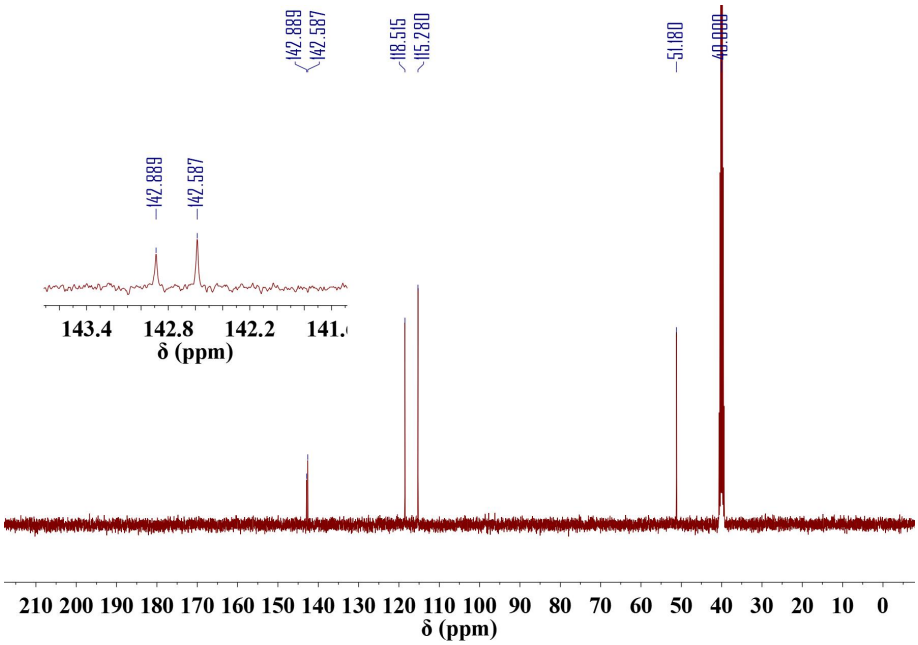

Fig. S16 ^{13}C NMR spectrum of **PA-NH$_2$** in DMSO-d$_6$.

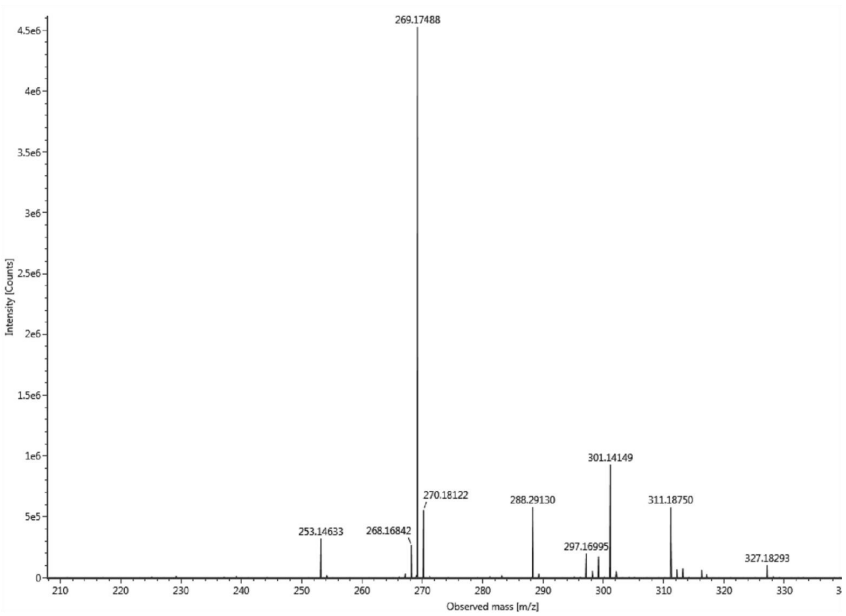

Fig. S17 HR-MS spectrum of **PA-NH$_2$**.

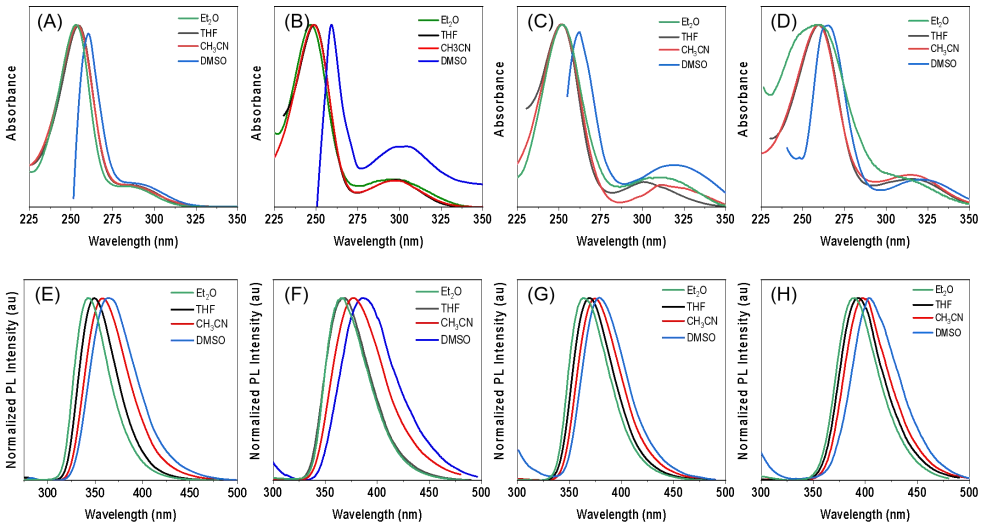

Fig. S18 Absorption spectra of (A) **PA-H**, (B) **PA-F**, (C) **PA-OCH$_3$**, and (D) **PA-NH$_2$** in varies of solution. Fluorescence spectra of (E) **PA-H**, (F) **PA-F**, (G) **PA-OCH$_3$**, and (H)**PA-NH$_2$** in varies of solution.

Table S1. The molar extinction coefficients of **PA**s.

PAs	ε_{THF} (×10^4)	ε_{H2O} (×10^4)	ε_{DMSO} (×10^4)	$\varepsilon_{Toluene}$ (×10^4)
PA-H	3.9 (250 nm)	1.9 (250 nm)	-	-
PA-F	3.2 (249 nm)	1.0 (249 nm)	-	-
PA-OCH$_3$	2.5 (252 nm)	1.2 (252 nm)	-	-
PA-NH$_2$	3.0 (260 nm)	1.2 (260 nm)	-	-
PA-CN	3.4 (297 nm)	1.3 (297 nm)	-	-
PA-Py$^+$	-	-	2.9 (419 nm)	1.7 (419 nm)

Table S2. The fluorescence lifetime (τ) of **PA**s in different states.

PAs	τ_{THF} (ns)	τ_{H2O} (ns)	τ_{DMSO} (ns)	$\tau_{Toluene}$ (ns)
PA-H	2.5030	-	-	-
PA-F	3.7216	-	-	-
PA-OCH$_3$	3.6154	-	-	-
PA-NH$_2$	4.8897	-	-	-
PA-CN	5.5948	0.7873 (352 nm) 3.2654 (462 nm)	-	-
PA-Py$^+$	-	-	0.5916	4.6342

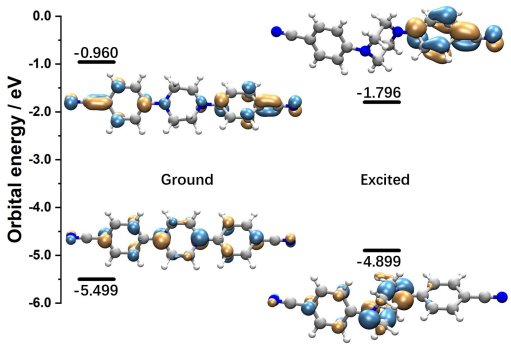

Fig. S19 The HOMO and LUMO of **PA-CN** at the minimum energy structures of the electronic ground and excited states.

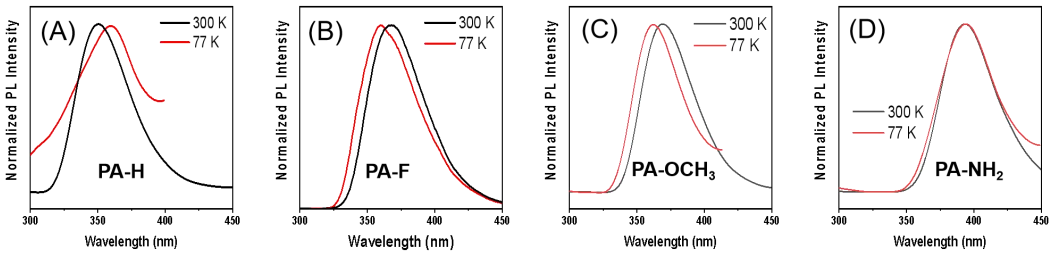

Fig. S20 The normalized PL intensity of (A) **PA-H**, (B) **PA-F**, (C) **PA-OCH$_3$**, and (D) **PA-NH$_2$** at 300 K and 77 K. (c_{PA} = 10 μM)

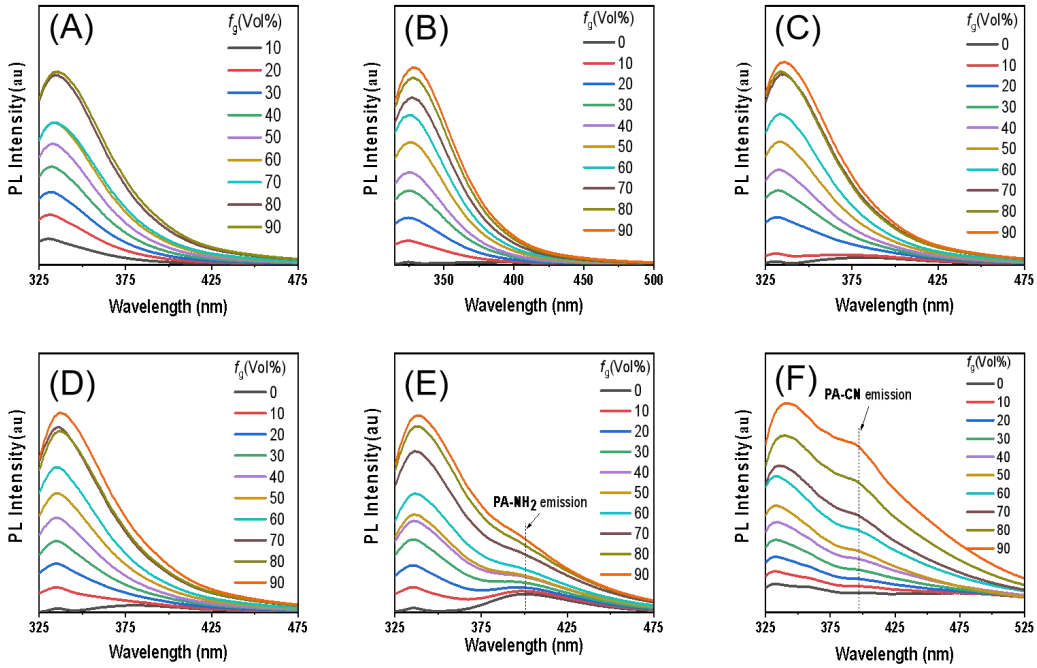

Fig. S21 (A) Emission spectra of blank control group with excitation wavelength = 300 nm. Emission spectra of (B) **PA-H**, (C) **PA-F**, (D) **PA-OCH$_3$**, (E) **PA-NH$_2$**, and (F) **PA-CN** in mixtures of MeOH/glycerol with different f_g (Vol%). (c_{PA} = 1 μM)

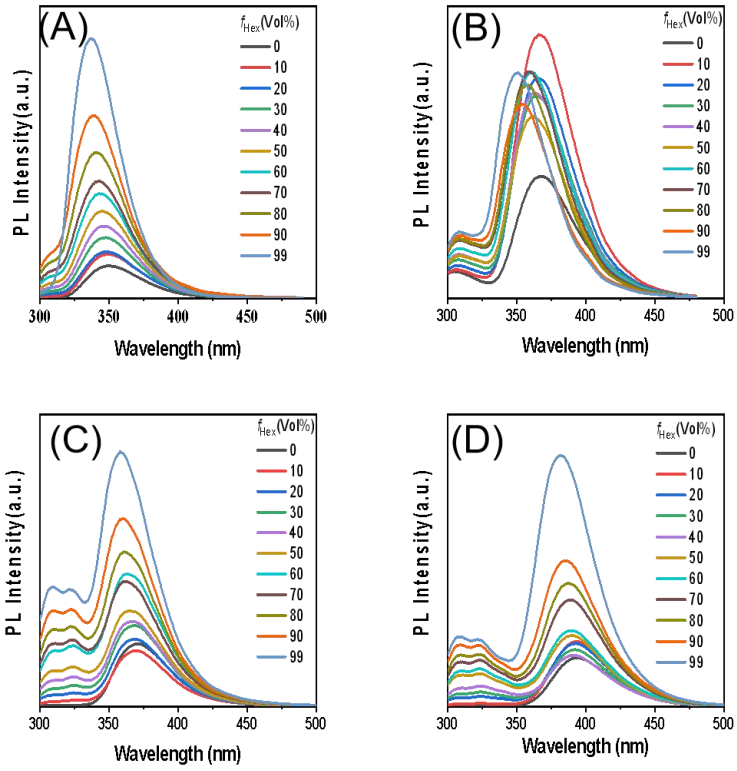

Fig. S22 Emission spectra of (A) **PA-H**, (B) **PA-F**, (C)**PA-OCH$_3$**, and (D) **PA-NH$_2$** in mixtures of THF/Hexane with different f_{Hex} (c_{PA} = 10 μM).

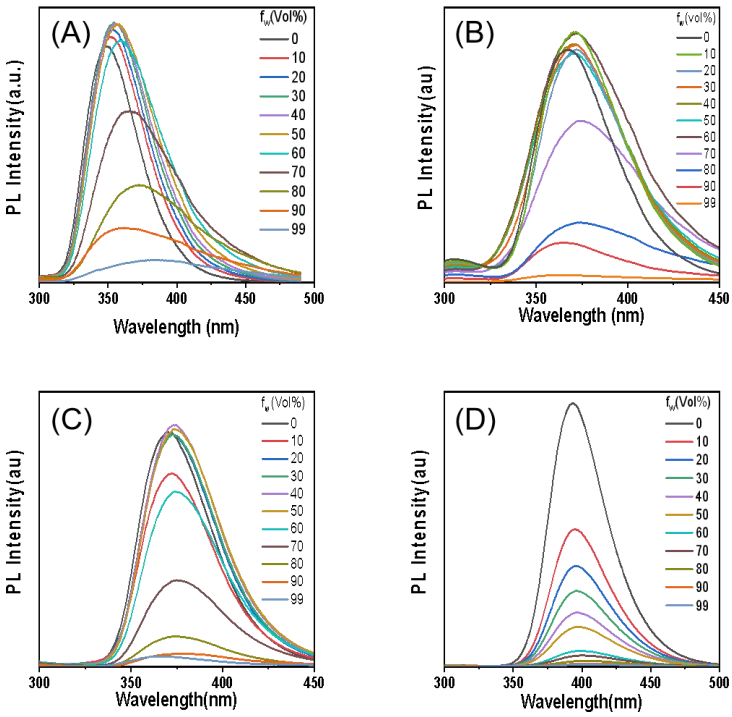

Fig. S23 Emission spectra of (A) **PA-H**, (B) **PA-F**, (C) **PA-OCH$_3$**, and (D) **PA-NH$_2$** in mixtures of THF/water with different f_w (c_{PA} = 10 μM).

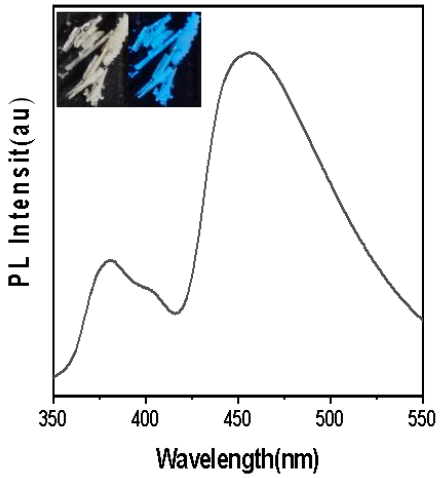

Fig. S24 Emission spectra of **PA-CN** crystal. Inset: images of **PA-CN** crystal under day light and 254 nm UV irradiation.

Table S3. The fluorescence quantum yields (QY) of **PA**s in different states.

PAs	QY_{THF} (%)	QY_{Water} (%)	QY_{DMSO} (%)	$QY_{Toluene}$ (%)
PA-H	10.68	2.43	-	-
PA-F	9.7	1.89	-	-
PA-OCH_3	15.42	3.3	-	-
PA-NH_2	7.23	0.43	-	-
PA-CN	12.65	22.74	-	-
PA-Py^+	-	-	0.57	14.24

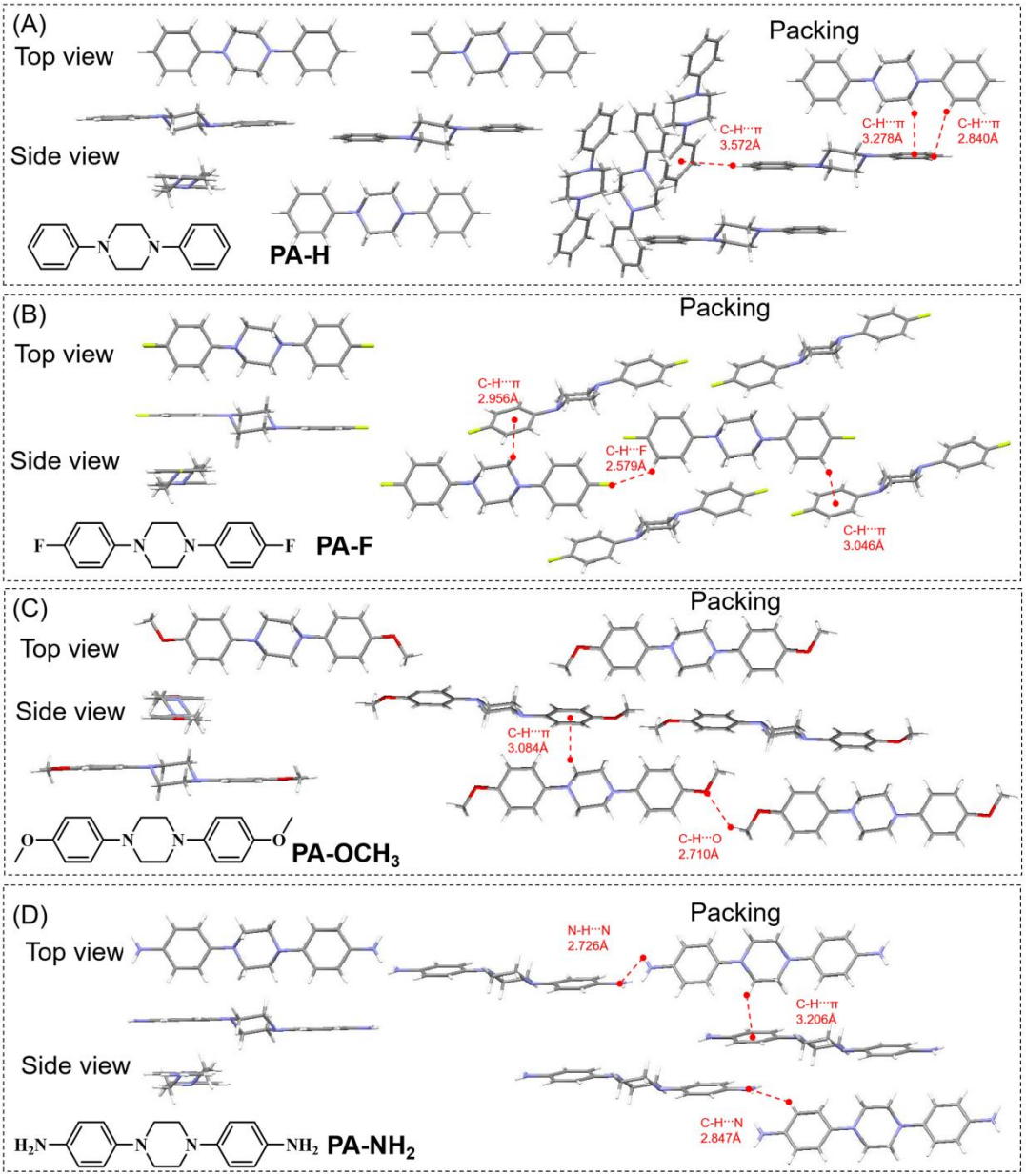

Fig. S25 Crystal information, including unimolecular conformation, dihedral angles, and intermolecular interactions (e.g. C−H···N, C−H···*π*, *π*···*π*), of (A) **PA-H**, (B) **PA-F**, (C) **PA-OCH$_3$**, and (D) **PA-NH$_2$**.

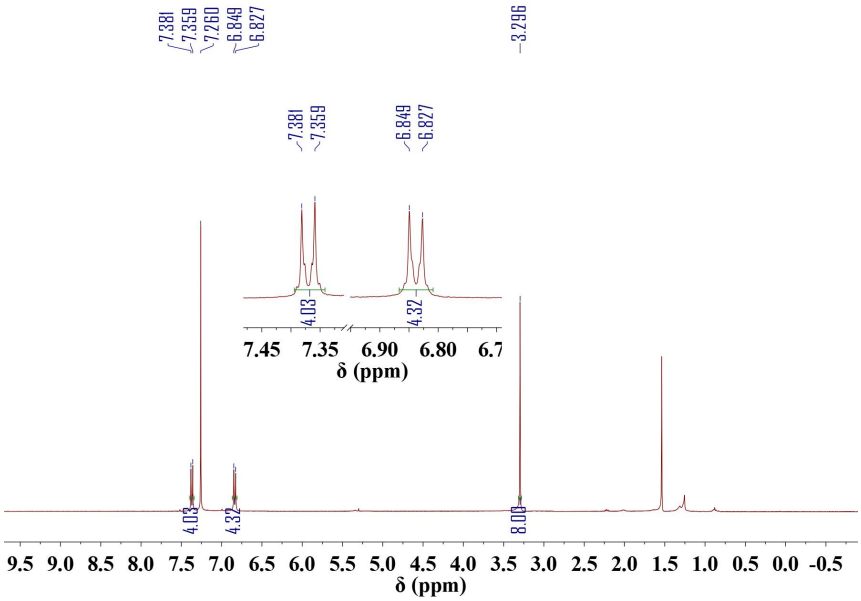

Fig. S26 ^{1}H NMR spectrum of **PA-Br** in $CDCl_3$.

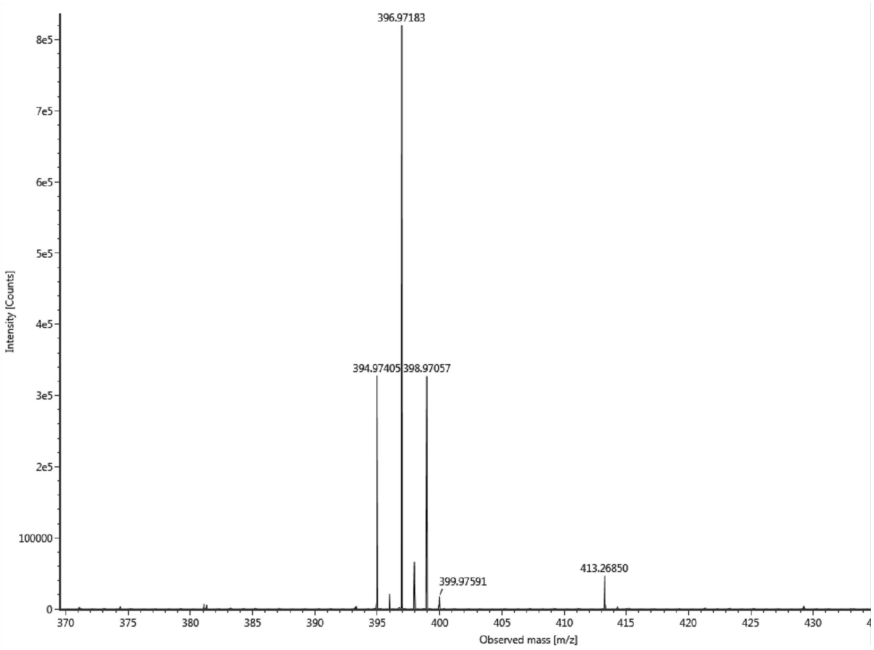

Fig. S27 HR-MS spectrum of **PA-Br**.

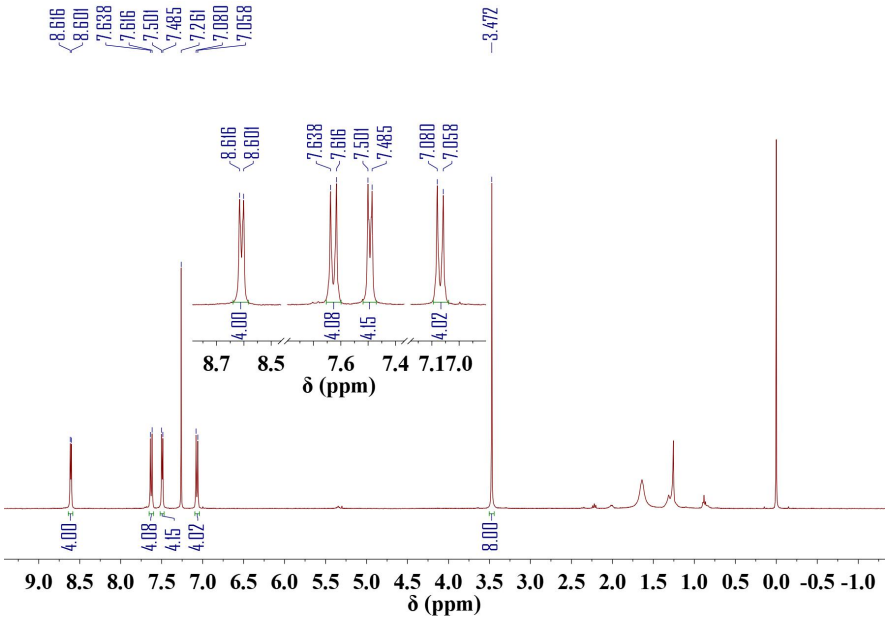

Fig. S28 ^{1}H NMR spectrum of **PA-Py** in $CDCl_3$.

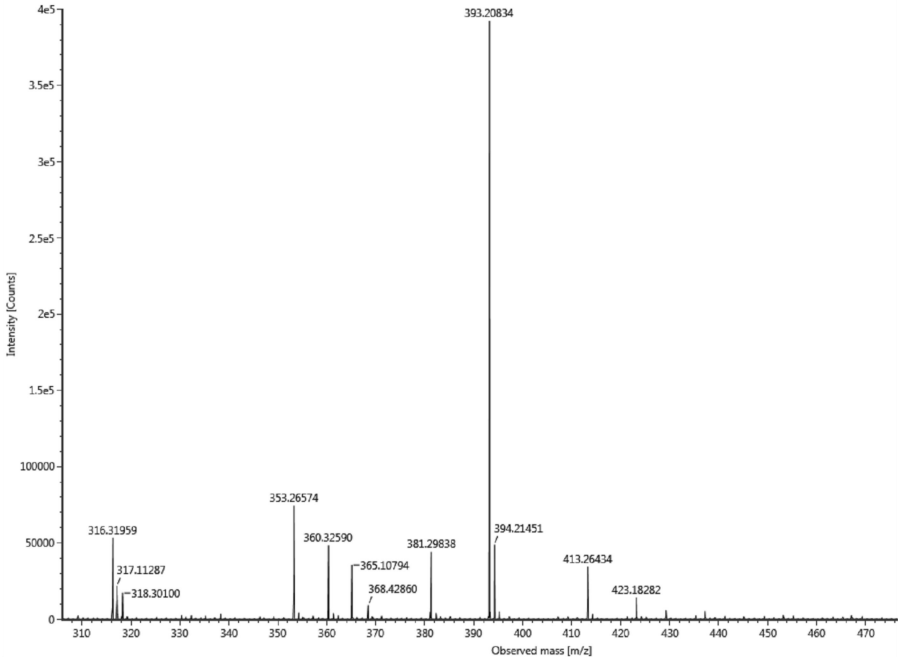

Fig. S29 HR-MS spectrum of **PA-Py**.

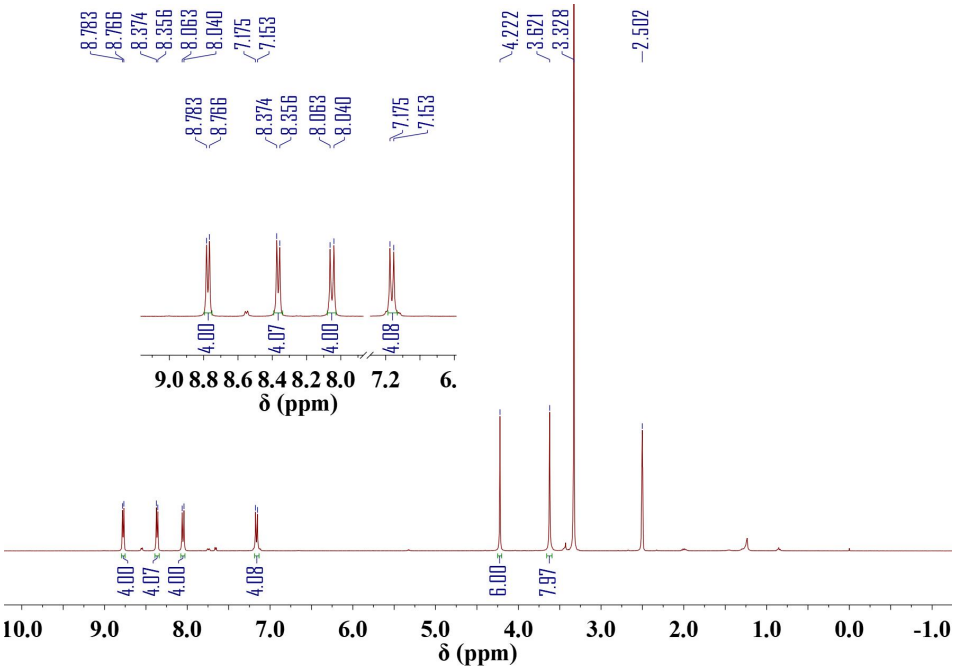

Fig. S30 ^{1}H NMR spectrum of **PA-Py⁺** in DMSO-*d*6.

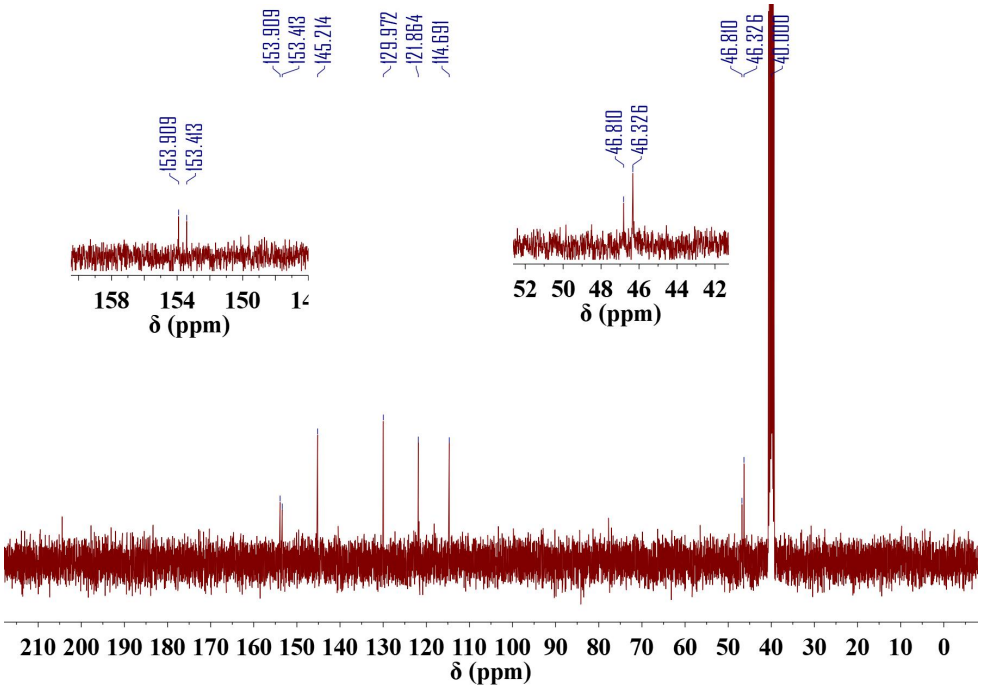

Fig. S31 ^{13}C NMR spectrum of **PA-Py⁺** in DMSO-*d*6.

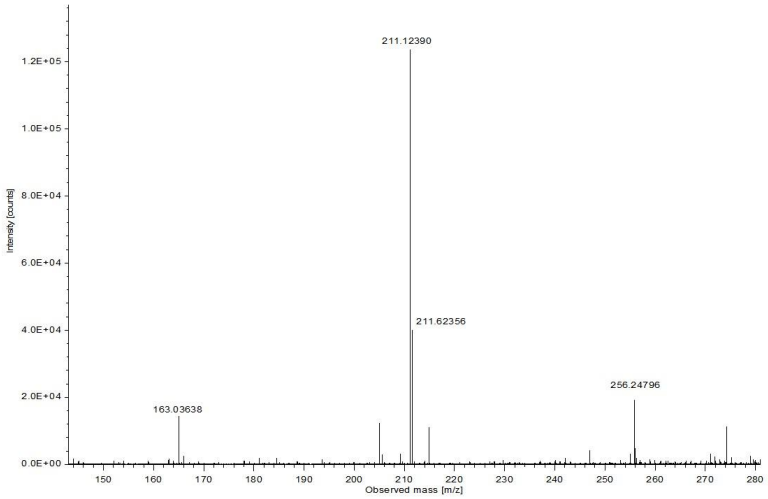

Fig. S32 HR-MS spectrum of **PA-Py⁺**.

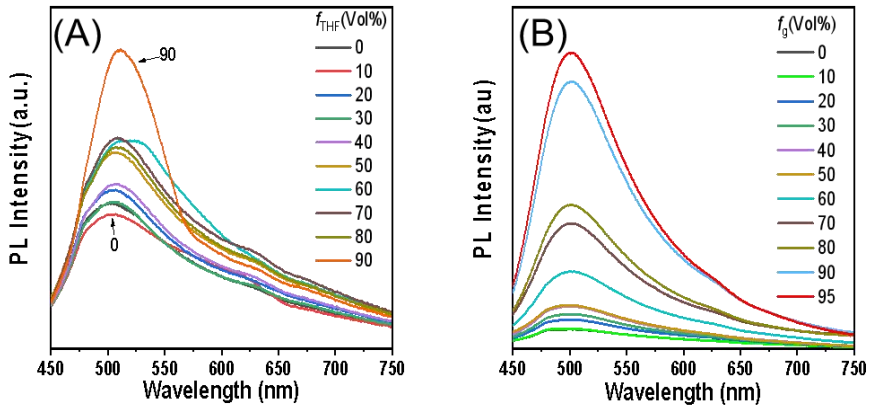

Fig. S33 (A) Emission spectra of **PA-Py⁺** in mixtures of MeOH/THF with different f_{THF} ($c_{PA\text{-}Py+}$ = 10 μM). (B) Emission spectra of **PA-Py⁺** in mixtures of MeOH/glycerol with different f_g (Vol%).($c_{PA\text{-}Py+}$ = 10 μM)

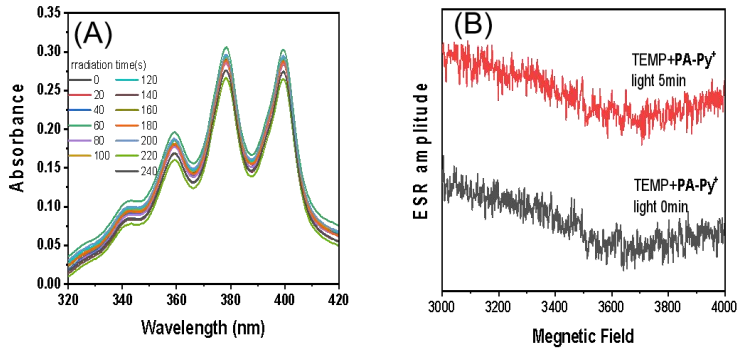

Fig. S34 (A) UV/Vis absorption spectra of ABDA (c_{ABDA} = 40 μM) in **PA-Py⁺** ($c_{PA\text{-}Py+}$ = 10 μM) solution under white light irradiation. (B) ESR spectra to detect $^1O_2$ generation from **PA-Py⁺** under irradiation, using TEMP as the spin-trap agent.

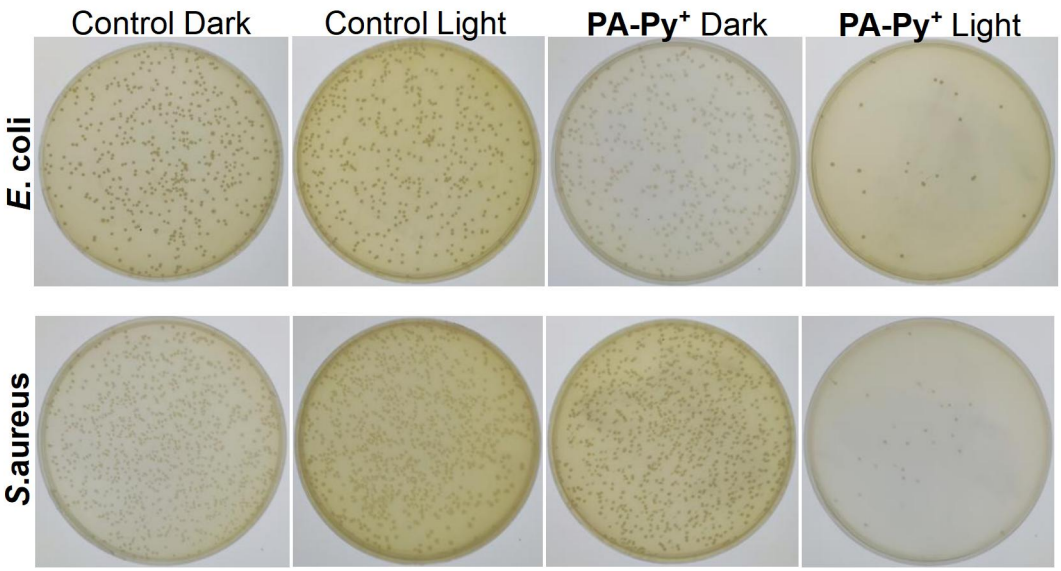

Fig. S35 Plate photographs of *E.* coil and *S.* aureus on agar plate supplemented with or without **PA-Py⁺** ($C_{PA\text{-}Py+}$ = 10 μM) in darkness or upon white light irradiation and then grown overnight.

Table S4. Single crystal data of **PA-H**, **PA-F**, **PA-OCH₃**, **PA-NH₂**, **PA-CN**, and **DMABN**.

Compound	**PA-H**	**PA-F**	**PA-OCH$_3$**	**PA-NH$_2$**	**PA-CN**	**DMABN**
Identification code	exp_7878	exp_7770	exp_7936	exp_7935	exp_7932	exp_8224
Empirical formula	$C_{16}H_{18}N_2$	$C_{16}H_{16}F_2N_2$	$C_{18}H_{22}N_2O_2$	$C_{16}H_{20}N_4$	$C_{18}H_{16}N_4$	$C_9H_{10}N_2$
Formula weight	238.32	274.31	298.38	268.36	288.35	146.19
Temperature / K	239.95(10)	113.50(10)	117.4(3)	117.7(6)	117.1(8)	117.80(10)
Crystal system	orthorhombic	monoclinic	monoclinic	monoclinic	monoclinic	monoclinic
Space group	Pbca	$P2_1/c$	$P2_1/n$	$P2_1/c$	$P2_1/c$	$P2_1/c$
a / Å	8.5407(8)	8.4198(9)	7.7608(9)	12.305(6)	4.0268(2)	7.105(5)
b / Å	8.5954(10)	5.6543(6)	8.3096(9)	5.6820(10)	11.5604(8)	7.513(6)
c / Å	18.058(2)	14.1818(11)	11.9313(12)	10.771(4)	15.2182(10)	15.636(15)
α/°	90	90	90	90	90	90
β/°	90	101.313(9)	103.196(10)	113.87(6)	93.647(5)	88.918(6)
γ/°	90	90	90	90	90	90
Volume / Å^3	1325.6(3)	662.05(11)	749.13(14)	688.7(5)	1413.51(16)	834.80(12)
Z	4	2	2	2	4	4
ρ_{calc} / mg mm^{-3}	1.194	1.376	1.323	1.294	1.355	1.163
μ / mm^{-1}	0.071	0.102	0.087	0.08	0.084	0.071
F(000)	512	288	320	288	608	312
Crystal size / mm^3	0.34 × 0.29 × 0.14	0.26 × 0.23 × 0.22	0.35 × 0.30 × 0.23	0.37 × 0.35 × 0.01	0.33 × 0.28 × 0.24	0.21 × 0.14 × 0.04

2Θ range for data collection	6.56 to 51.98°	6.88 to 51.96°	7.28 to 51.94°	7.24 to 51.96°	6.42 to 52°	7.52 to 52°
Index ranges	$-10 \leq h \leq 9$, $-7 \leq k \leq 10$, $-22 \leq l \leq 21$	$-10 \leq h \leq 9$, $-6 \leq k \leq 6$, $-17 \leq l \leq 16$	$-9 \leq h \leq 9$, $-10 \leq k \leq 10$, $-14 \leq l \leq 14$	$-15 \leq h \leq 15$, $-6 \leq k \leq 6$, $-13 \leq l \leq 11$	$-4 \leq h \leq 4$, $-14 \leq k \leq 14$, $-37 \leq l \leq 36$	$-8 \leq h \leq 8$, $-9 \leq k \leq 9$, $-19 \leq l \leq 17$
Reflections collected	5437	2438	3046	3631	21049	3504
Independent reflections	1295[R(int) = 0.0636 (inf-0.9Å)]	1268[R(int) = 0.0328 (inf-0.9Å)]	1434[R(int) = 0.0441 (inf-0.9Å)]	1319[R(int) = 0.0993 (inf-0.9Å)]	5435[R(int) = 0.0450 (inf-0.9Å)]	1610[R(int) = 0.0714(inf-0.9Å)]
Data	1295	1268	1434	1319	5435	1610
restraints	0	0	0	0	61	0
parameters	83	91	101	92	398	102
Goodness-of-fit on F^2	1.058	1.079	1.047	1.041	1.078	1.027
Final R indexes [I>2σ (I) i.e. F_o>4σ (F_o)]	R_1 = 0.0546, wR_2 = 0.1094	R_1 = 0.0483, wR_2 = 0.1112	R_1 = 0.0525, wR_2 = 0.1023	R_1 = 0.0973, wR_2 = 0.2299	R_1 = 0.0417, wR_2 = 0.1045	R_1 = 0.0642, wR_2 = 0.1089
Final R indexes [all data]	R_1 = 0.1096, wR_2 = 0.1396	R_1 = 0.0634, wR_2 = 0.1230	R_1 = 0.0809, wR_2 = 0.1233	R_1 = 0.1789, wR_2 = 0.2899	R_1 = 0.0479, wR_2 = 0.1209	R_1 = 0.1518, wR_2 = 0.1588
Largest diff. peak/hole / e $Å^{-3}$	0.136/-0.128	0.191/-0.231	0.216/-0.224	0.370/-0.306	0.182/-0.219	0.205/-0.226
Flack Parameters	N	N	N	N	0(9)	N
Completeness	0.9957	0.997	0.9951	0.9912	0.996	0.9969

References

[1] Xu, S.; He, T., Li, J., Huang, Z., Hu, C. Enantioselective synthesis of D-lactic acid via chemocatalysis using MgO: Experimental and molecular-based rationalization of the Triose's reactivity and preliminary insights with raw biomass. Appl. Catal. B: Environ. **2021**, 292, 120145.

[2] Bauernschmitt, R.; Ahlrichs, R. Treatment of electronic excitations within the adiabatic approximation of time dependent density functional theory. Chem. Phys. Lett. **1996**, 256: 454–464.

[3] Casida, M. E.; Jamorski, C.; Casida, K. C.; Salahub, D. R. Molecular excitation energies to high-lying bound states from time-dependent density-functional response theory: Characterization and correction of the time dependent local density approximation ionization threshold. J. Chem. Phys. **1998**, 108: 4439–4449.

[4] Stratmann, R. E.; Scuseria, G. E.; Frisch, M. J. An efficient implementation of time-dependent density functional theory for the calculation of excitation energies of large molecules. J. Chem. Phys., **1998**, 109: 8218–8224.

[5] Van Caillie, C; Amos, R. D. Geometric derivatives of excitation energies using SCF and DFT. Chem. Phys. Lett., **1999**, 308: 249–255.
[6] Van Caillie, C.; Amos, R. D. Geometric derivatives of density functional theory excitation energies using gradient-corrected functionals. Chem. Phys. Lett. **2000**, 317: 159–164.
[7] Furche, F.; Ahlrichs, R. Adiabatic time-dependent density functional methods for excited state properties. J. Chem. Phys., **2002**, 117: 7433–7447.
[8] Becke, A. D. Density-functional thermochemistry. III. The role of exact exchange. J. Chem. Phys. **1993**, 98, 5648−5652.
[9] Lee, C., Yang, W., Parr, R. G. Development of the Colle-Salvetti correlation-energy formula into a functional of the electron density. Phys. Rev. B. **1988**, 37, 785−789.
[10] Grimme, S.; Stephan, E.; Lars, G. Effect of the damping function in dispersion corrected density functional theory. J. Comput. Chem. **2011**, 32, 1456−1465.
[11] Weigend, F.; Ahlrichs, R. Balanced basis sets of split valence, triple zeta valence and quadruple zeta valence quality for H to Rn: Design and assessment of accuracy. Phys. Chem. Chem. Phys. **2005**, 7, 3297−3305.
[12] Weigend, F. Accurate coulomb-fitting basis sets for H to Rn. Phys. Chem. Chem. Phys. **2006**, 8, 1057−1065.
[13] Frisch, M. J.; Trucks, G. W.; Schlegel, H. B.; Scuseria, G. E.; Robb, M. A.; Cheeseman, J. R.; Scalmani, G.; Barone, V.; Mennucci, B.; Petersson, G. A.; Nakatsuji, H.; Caricato, M.; Li, X.; Hratchian, H. P.; Izmaylov, A. F.; Bloino, J.; Zheng, G.; Sonnenberg, J. L.; Hada, M.; Ehara, M.; Toyota, K.; Fukuda, R.; Hasegawa, J.; Ishida, M.; Nakajima, T.; Honda, Y.; Kitao, O.; Nakai, H.; Vreven, T.; Montgomery Jr, J. A.; Peralta, J. E.; Ogliaro, F.; Bearpark, M. J.; Heyd, J.; Brothers, E. N.; Kudin, K. N.; Staroverov, V. N.; Kobayashi, R.; Normand, J.; Raghavachari, K.; Rendell, A. P.; Burant, J. C.; Iyengar, S. S.; Tomasi, J.; Cossi, M.; Rega, N.; Millam, N. J.; Klene, M.; Knox, J. E.; Cross, J. B.; Bakken, V.; Adamo, C.; Jaramillo, J.; Gomperts, R.; Stratmann, R. E.; Yazyev, O.; Austin, A. J.; Cammi, R.; Pomelli, C.; Ochterski, J. W.; Martin, R. L.; Morokuma, K.; Zakrzewski, V. G.; Voth, G. A.; Salvador, P.; Dannenberg, J. J.; Dapprich, S.; Daniels, A. D.; Farkas, Ö.; Foresman, J. B.; Ortiz, J. V.; Cioslowski, J.; Fox, D. J. Gaussian 09, Revision D.01. **2009**, Gaussian, Inc., Wallingford, CT, USA.
[14] Marenich, A. V.; Cramer, C. J.; Truhlar, D. G. Universal solvation model based on solute electron density and on a continuum model of the solvent defined by the bulk dielectric constant and atomic surface tensions. J. Phys. Chem. B **2009**, 113, 6378−6396.